

pubs.acs.org/estair Article

Amplification of Surface Ozone by the Aerosol Direct Effect under COVID-19 Lockdown in Shanghai, China

Zhixu Sun, Jiani Tan, Murnira Othman, Yangjun Wang, Juntao Huo, Maggie Chel Gee Ooi, Ling Huang, Cheng Huang, Mohd Talib Latif, Joshua S. Fu, and Li Li*



Cite This: ACS EST Air 2025, 2, 2147-2161



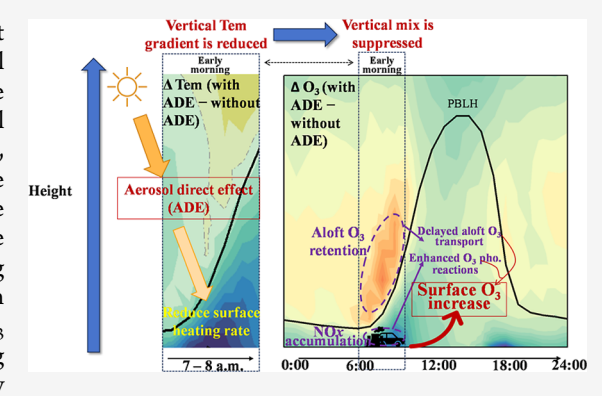
ACCESS I

III Metrics & More

Article Recommendations

s Supporting Information

ABSTRACT: Elevated surface ozone (O_3) concentrations present substantial risks to public health, ecosystem productivity, and global climate change. Shanghai implemented a citywide lockdown to control the spread of COVID-19 during April to May of 2022, leading to substantial reduction in air pollutant emissions. The surface O_3 concentrations, however, increased by 3–10 ppb compared to 2021 in most areas of the Yangtze River Delta (YRD) region. This phenomenon presented a unique real-world experiment on air pollution management. Here, we integrate observational data and two-way online meteorology—air quality modeling to investigate the causes of this unexpected O_3 increase, with a focus on elaborating the interaction between the aerosol direct effect (ADE) and O_3 formation. Results showed that aerosol loading suppressed early morning vertical mixing, enhancing photochemical reactivity below the boundary



layer and delaying upward O_3 transport. This ADE contributed an average 10.8 ppb increase in O_3 concentrations during pollution episodes (O_3 concentration >100 ppb), with emission-reduction-induced ADE raising O_3 by 6.2 ppb in Shanghai and 3.5 ppb in Jiangsu. In addition, vertical transport contributed to -4 ± 1 ppb changes in O_3 , although the surface meteorological conditions in Shanghai were favorable for O_3 photochemical formation. In contrast, meteorology dominated the O_3 increase (5 ± 3 ppb) in northwestern YRD. The lockdown caused a 10% higher reduction in nitrogen oxides than volatile organic compounds, leading to O_3 increases of 9 ± 1 ppb in Shanghai and 5 ± 2 ppb in southern Jiangsu. These findings highlight the risk of O_3 increases resulting from imbalanced changes in the precursors, aerosols, and meteorology. We suggest taking into consideration the effect of aggregation of O_3 by ADE when designing air quality management strategies.

KEYWORDS: surface ozone, aerosol direct effect, WRF-CMAQ online modeling, COVID-19

1. INTRODUCTION

Ground-level ozone (O_3) is a significant environmental challenge due to its impacts on air quality, human health, ecosystems, and climate change, $^{1-3}$ which has attracted global attention. 4 O_3 is formed through nonlinear photochemical reactions between volatile organic compounds (VOCs) and nitrogen oxides (NOx) in the presence of solar radiation. 5 O_3 is also influenced by regional transport, as emissions from upwind areas can significantly affect the O_3 concentrations of the corresponding gases downwind. Therefore, meteorological conditions, precursor emissions, and photochemical reactions directly affect the formation of O_3 . Moreover, the role of aerosols in O_3 formation cannot be overlooked, as they are believed to cool the surface atmosphere via aerosol direct effects (ADE) and alter atmospheric oxidation capacity by changing photolysis rates and heterogeneous reactions. $^{6-8}$

A growing body of research has investigated O₃ concentration responses to COVID-19 lockdowns across different regions, revealing that reductions in primary emissions can have complex and sometimes counterintuitive effects on

secondary pollutants like O₃. For example, studies in Beijing, Europe, and the United States reported either increases or negligible changes in O₃ despite reduced NOx emissions, depending on regional VOC sensitivity and meteorological conditions. ^{10–12} In addition, recent studies have shown that such aerosol reductions during the COVID-19 lockdown can significantly enhance surface O₃ through ADE. For instance, Zhu et al. (2021)¹³ demonstrated that a sharp decline in aerosol concentrations weakened ADE and consequently increased O₃ levels over China. Similarly, Menut et al. (2022)¹⁴ reported that during Europe's lockdown, reduced aerosols enhanced surface solar radiation and photochemistry. These findings suggested that the ADE mechanism may have

Received: April 19, 2025
Revised: September 2, 2025
Accepted: September 3, 2025
Published: September 11, 2025





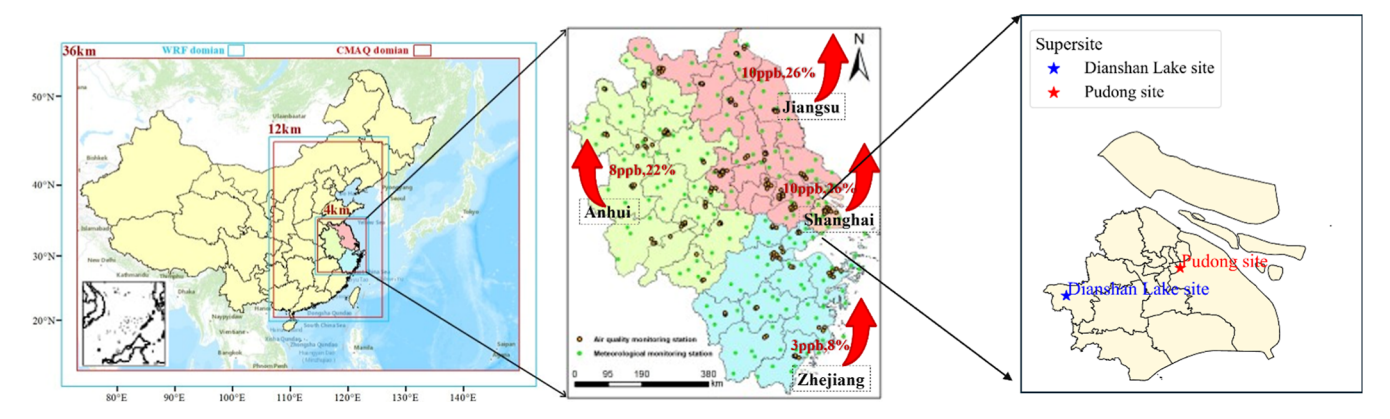


Figure 1. Model domain. The innermost domain on the left figure is the main research area for the YRD. The domain of WRF is three grids larger on each side than CMAQ to fully cover it. The middle figure shows a more refined YRD city division, where orange dots represent national air quality monitoring stations and green dots represent national meteorological monitoring stations. The right figure shows locations of the Pudong supersite and Dianshan Lake supersite operated by the Shanghai Environmental Monitoring Center.

played a critical role in modulating the O_3 variations during the COVID-related emission changes. Yet, detailed analysis of this mechanism under different levels of precursors and meteorological conditions remains limited.

The Yangtze River Delta (YRD) region, encompassing Shanghai, Jiangsu, Anhui, and Zhejiang provinces, is one of the most economically developed city clusters in eastern China and one of the areas with intensive emissions of air pollutants. Shanghai, the economic hub of China, implemented a citywide lockdown in spring 2022 (April to May) to control the rapid spread of COVID-19, 15-17 resulting in nearly 50% reduction in NOx and 40% drop in VOCs emissions but observed 10 ± 2 ppb (16-26%) increase in surface O₃ levels compared to 2021. 18,19 Simultaneously, the aerosol optical depth (AOD) was also observed to decrease by 40% in Shanghai. This unexpected increase in the level of O₃ has drawn substantial research interest. Previous studies have explored the reasons behind Shanghai's Spring 2022 O₃ surge, 15[±]21 concluding that meteorology was not the primary driver but rather the more pronounced reduction in NOx compared to VOC emissions due to lockdown restrictions on industrial and mobile sources. While these studies have enhanced our understanding of O₃ formation in Shanghai, several critical aspects remain unexplored in this unique case. First, existing analyses of meteorology and air pollution have primarily relied on monthly averages at the surface level, lacking a comprehensive threedimensional perspective that accounts for vertical meteorological changes and transport of the O₃. Second, the increase in the level of O₃ was not confined to Shanghai; considerable increases in the level of O3 were also observed in Anhui and Jiangsu. Notably, southern Jiangsu, with its close economic ties to Shanghai, experienced substantial anthropogenic emission reductions but saw a marked increase in the level of O₃. In contrast, anthropogenic emissions in Anhui remained largely unaffected by Shanghai's lockdown. Third, despite the significant reduction in aerosol emissions in Shanghai, their impact on the formation of O₃ has yet to be fully elucidated. Even beyond this specific case, previous studies on ADE have typically focused on average concentrations, with limited indepth exploration of the underlying mechanisms. The regional changes in the concentration of O₃ across the YRD region have thus not been fully understood.

The 2022 Spring lockdown in Shanghai offers a valuable real-world experiment for the control of pollution by O_3 and its

corresponding precursors, akin to future efforts to reduce anthropogenic emissions. It also serves as a unique case study to better understand the nonlinear mechanisms of O_3 formation and the feedback among aerosol reductions, meteorological changes, and the effects of O_3 fluctuations. In this study, we employed surface and vertical measurements, satellite data, and an online coupled meteorology—chemistry model to comprehensively explore the causes behind the increase of O_3 in Shanghai and the surrounding YRD region. We particularly focus on unraveling the mechanism of ADE on the effect of O_3 changes. The results of this study could provide valuable insights for future O_3 pollution control strategies, especially in the context of climate change and ongoing efforts to reduce anthropogenic emissions.

2. METHODOLOGY

2.1. Data. Surface observational data, which included hourly concentrations of O₃, nitrogen dioxide (NO₂), and fine particulate matter (PM_{2.5}), were from the National Air Quality Monitoring Stations operated by the China National Environmental Monitoring Centre (https://quotsoft.net/air, last access 06/08/2024). Observed PM_{2.5} chemical compositions including sulfate (SO₄²⁻), nitrate (NO₃⁻), ammonium (NH₄⁺), organic carbon (OC), and elemental carbon (EC) concentrations at the Dianshan lake supersite, ground radar data including planetary boundary layer height (PBLH), and O₃ vertical profile at the Pudong monitoring site were operated by the Shanghai Environmental Monitoring Center. Satellitebased observational data included AOD from the Himawari-8 satellite's reprocessed final-level (L3) data set (https://earth. jaxa.jp/en/, last access 09/18/2024). The formaldehyde (HCHO) and NO₂ column concentrations were obtained from the Sentinel-5 L3 satellite data (https://sentinels. copernicus.eu/web/sentinel/missions/sentinel-5, last access 06/10/2024), with preprocessing conducted using Google Earth Engine (https://earthengine.google.com, last access 12/ 06/2024). The surface temperature (Tem), relative humidity (RH), precipitation (Pre), and wind speed (WS) were downloaded from the China Meteorological Administration (http://data.cma.cn, last access 06/08/2024). Data from the fifth generation ECMWF atmospheric reanalysis (ERA5, https://www.ecmwf.int/en/forecasts/dataset/ecmwfreanalysis-v5, last access 01/18/2025), including surface and vertical Tem, surface net solar radiation (SSR), RH, total cloud

Table 1. Scenario Design for WRF-CMAQ

			emissi	on	aerosol effect		
case	WRF-CMAQ modeling system	meteorology	anthropogenic emissions	biogenic emissions	aerosol direct effect	heterogeneous reaction	photolysis
Base 1-2022	online	2022	2022	2022	$\sqrt{}$		
Base 2-2021	online	2021	2021	2021	$\sqrt{}$	$\sqrt{}$	$\sqrt{}$
Sce.1-2021M2022E	online	2021	2022	2022	$\sqrt{}$	$\sqrt{}$	$\sqrt{}$
Sce.2-2022M2021B	online	2022	2022	2021	$\sqrt{}$	$\sqrt{}$	
Sce.3-2022M2021A	online	2022	2021	2022	$\sqrt{}$	$\sqrt{}$	
Sce.4-ADE_a	offline	2022	2022	2022	×	$\sqrt{}$	$\sqrt{}$
Sce.5-Het_a	online	2022	2022	2022	$\sqrt{}$	×	$\sqrt{}$
Sce.6-Pho_a	online	2022	2022	2022	$\sqrt{}$	$\sqrt{}$	×
Sce.7-ADE_b	offline	2022	2021	2022	×	$\sqrt{}$	$\sqrt{}$
Sce.8-Het_b	online	2022	2021	2022	$\sqrt{}$	×	
Sce.9-Pho_b	online	2022	2021	2022	$\sqrt{}$	$\sqrt{}$	×

cover (TCC), and wind direction (WD), were also used in this study. Extensive cross-disciplinary studies have used ERAS data as a representation of the relatively real atmospheric field.^{22,23} We followed the methods of Garces et al. (2010)²⁴ and Junninen et al. (2004)²⁵ to conduct data quality control. Detailed information about these data and post-processing can be found in Text S1.

2.2. Model Configuration. The online coupled Weather Research and Forecasting (WRF) model (version 4.4, https:// www.mmm.ucar.edu/wrf-model-general, last access 04/12/ 2024) and the Community Multiscale Air Quality Model (CMAQ, version 5.4, https://www.epa.gov/cmaq, last access 04/12/2024) were utilized. The WRF model provided meteorological fields to CMAQ; the aerosol components and other air pollutant concentrations were predicted by CMAQ, and their optical properties were calculated by the coupler and transmitted to the WRF, where the radiative effects were calculated using the Rapid Radial Transfer Model for General Circulation Models. The feedback between aerosol and solar radiation is considered in the coupled online WRF-CMAQ modeling system. The process analysis (PA) module coupled within CMAQ is used to track the impact of specific chemical or physical processes on O₃ concentrations. Three nested domains with horizontal grid resolutions of 36, 12, and 4km are utilized for the online WRF-CMAQ modeling system (Figure 1). The inner 4 km domain covered the entire YRD, including three provinces and the Shanghai megacity (Figure 1). The chemical initial and boundary conditions for the CMAQ model were provided by the Whole Atmosphere Community Climate Model.²⁶ The WRF model setup used the Goddard shortwave radiation scheme, the Yonsei University Planetary Boundary Layer scheme, the Noah Multi Physics land surface model, and the Purdue Lin microphysics scheme, while CMAQ utilized the gas-phase chemical mechanism SAPRC07 and aerosol scheme Aero07. The simulation period was from March 15th to May 31st in both 2021 and 2022, with the first 15 days as spin-up time.

The emission inventories for both the 36 km and 12 km domains were derived from the multiresolution emission inventory model for climate and air pollution research (MEIC)²⁷ for the year 2020. For the simulation of the innermost domain, anthropogenic emission inventory was adopted from the studies by An et al. (2021)²⁸ and Huang et al. (2021)²⁹ with higher resolution and local emission information for the year 2017. To estimate the emissions for the years 2021 and 2022 in the YRD, we first scaled the 2021

emissions based on the variations in MEIC across different sectors from 2017 to 2021 (since MEIC does not provide publicly available 2021 emission inventory, we assume that emissions in 2021 will be similar to those in 2020). For the 2022 emissions, we first assumed 2021 emissions as the 2022 emissions without the lockdown and then projected the 2022 lockdown emissions based on the statistics of activity data in each province and city. Detailed anthropogenic emissions and reduction ratio due to lockdown can be found in Text S2 and Table S1. Biogenic emissions were estimated by the Model of Emissions of Gases and Aerosols from Nature (v3.2. https:// bai.ess.uci.edu/megan, last access 03/07/2024). The hourly biomass burning emissions data were provided by the Fire Inventory (FINN) from NCAR (https://www2.acom.ucar. edu/modeling/finn-fire-inventory-ncar, last access 12/12/ 2023).

2.3. Model Scenarios Design. The brute force method is used to determine the effects of varied factors affecting changes in the level of O_3 . A total of 9 scenarios were simulated in this study, which are listed in Table 1. We set up two base cases: one representing the actual lockdown scenario in 2022 (Base 1-2022) and another representing the normal scenario in 2021 (Base 2-2021). These cases were also used for conducting model performance evaluation.

Sce.1-2021M2022E is set up to estimate the impact of meteorological changes on O₃. The parameters used for the Sce.1-2021M2022E scenario run were identical to those of Base 1-2022, but they utilized meteorological conditions for year 2021. By comparing Sce.1-2021M2022E and Base 1-2022, we can effectively quantify the influence of meteorological conditions on O₃ variations. Two distinct scenarios to quantify the impacts of biogenic and anthropogenic emissions on O₃ changes, are defined as Sce.2-2022M2021B and Sce.3-2022M2021A. Sce.2-2022M2021B uses identical parameterization as Base 1-2022 but incorporates the biogenic emission data from 2021. Similarly, Sce.3-2022M2021A employs the same parameterization as Base 1-2022 but utilizes emissions without reduction, assuming no lockdown conditions.

To explore the impact of aerosols on the level of O₃, we conducted two series of modeling runs. In the first series, three model scenarios were run, including Sce.4-ADE_a (turning off ADE), Sce.5-Het_a (turning off aerosol-involved heterogeneous reactions), and Sce.6-Pho_a (turning off the impact of aerosols on photolysis rates). Each is similar to the Base 1-2022 but with specific processes disabled. By comparing the results of these three scenarios with those of Base 1-2022, we

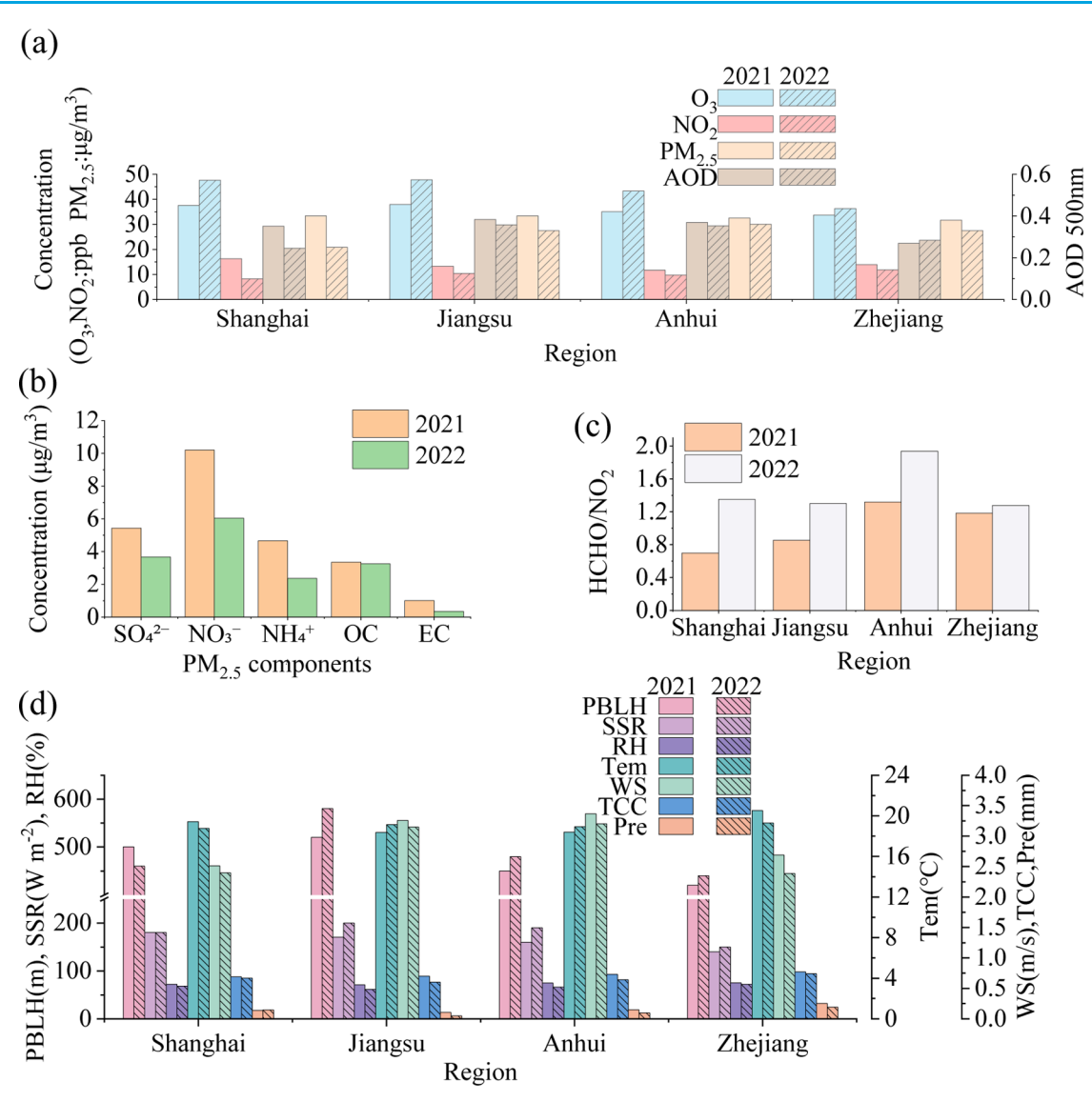


Figure 2. Comparisons of air pollutants and meteorological factors in the YRD region between 2021 and 2022 lockdown period. O_3 , NO_2 , and $PM_{2.5}$ data were obtained from ground observations (a), while $PM_{2.5}$ components ($SO_4^{\ 2^-}$, $NO_3^{\ -}$, $NH_4^{\ +}$, OC, and EC) were measured at the Dianshan Lake supersite (b). HCHO/NO₂ column concentrations were from Sentinel-5 satellite, and AOD were from Himawari-8 (c). RH, Tem, Pre, and WS data were sourced from ground observations, and other meteorological factors were sourced from ERAS (d).

quantified the individual contributions of the three aerosolrelated processes to the concentrations of the O₃ in 2022. In the second series, another three scenarios were performed, including Sce.7-ADE_b, Sce.8-Het_b, and Sce.9-Pho b, each of which is based on Sce.3-2022M2021A (i.e., using 2021 emissions with 2022 meteorology) but with the same specific processes turned off. The impact of aerosol emission reductions is the difference-in-difference (DID) between the contribution of aerosol to the level of O₃ in 2022 and the contribution in 2021. For example, to isolate the emissioninduced change in ADE's impact, we calculate (Base 1-2022-Sce.4-ADE a)—(Sec.3-2022M2021A-Sce.7-ADE b), where each pair isolates the ADE effect on O₃ under 2022 and 2021 emission scenarios, respectively. It is worth noting that in this study, the impact of reduced aerosols on the level of O₃ was assessed by comparing aerosol effects under different aerosol concentrations and O3 precursor emission scenarios (corresponding to 2022 and 2021 emissions) rather than merely altering aerosol concentrations. This approach better

reflects real annual variations, as isolating aerosol reductions is almost impossible due to their complex sources and secondary formation processes.

2.4. Model Performance Evaluation. Surface observational data and supplemented ERA5 data were used to evaluate the WRF-CMAQ model's performance on a three-dimensional scale. Meteorological evaluation parameters included Tem, RH, Pre, WS, and SSR, while surface air pollutant evaluation factors included the level of O₃ and PM_{2.5}. In the vertical dimension, meteorological evaluation parameters include temperature profiles and PBLH, and air pollutant evaluation factors include O₃ vertical profiles, HCHO/NO₂ column concentrations, and AOD. The benchmarks for evaluating O₃, PM_{2.5}, and meteorological parameters were based on Huang et al. (2024),³⁰ Huang et al. (2021),³¹ and Emery et al. (2001),³² respectively. Overall, the evaluation metrics selected include mean bias (MB), normalized mean bias (NMB), normalized mean error (NME), and correlation (R). Two baseline scenarios, Base 1-2022 and Base 2-2021,

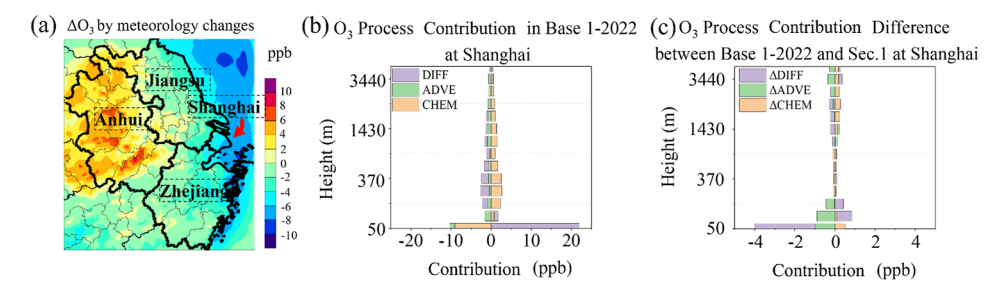


Figure 3. Meteorology-induced changes in O₃ concentration. (a) changes in O₃ concentration caused by meteorological changes in YRD. (b) contribution to O₃ from chemical, advection, and diffusion processes in the Base 1-2022 scenario. (c) difference between the Base 1-2022 scenario and Sce.1-2021M2022E scenario in O₃ contribution from chemical, advection, and diffusion processes. Chemical, advection, and diffusion processes were labeled CHEM, ADVE, and DIFF, respectively.

corresponding to the baseline conditions for 2022 and 2021, were used for model performance evaluation.

We first describe the evaluation of surface variables. For meteorology (Table S2), the performance of various parameters such as Tem, RH, and WS in different years in YRD was better than the recommended standards.³² The temperature's MB ranged from -2.4 to 0.7, with R higher than 0.92 and NME ranging between 6.3 and 14.3%. The RH's MB ranged from -6 to 2.8, with R > 0.93 and NME ranged from 4.5 to 13%. The WS's MB ranges from -0.33 to -0.37, with R ranging from 0.73 to 0.91 and NME ranging from 17 to 20%, except for Shanghai, where NME was 30%. The ERA5 data provided additional surface meteorological validation for the entire YRD, and WRF-CMAQ well simulated Tem, RH, and SSR for 2021 and 2022 and effectively captured meteorological changes between 2021 and 2022 (Figure S1). For O₃ (Table S2 and Figure S1), compared with ground-based observations, the MB values in YRD for 2022 (Table S2a) ranged from -2 to -1.3, with R ranging from 0.73 to 0.85 and NMB ranging from −4 to 4.9%. For 2021 (Table S2b), MB ranged from −0.1 to 1.5 ppb, R ranged from 0.72 to 0.81, and NMB ranged from -0.9 to 4.4%. All indicators were significantly better than the recommended benchmarks.³⁰ The NME values of O₃ for 2021 and 2022 ranged from 9.9 to 16%, slightly weaker than those for other parameters. The model simulation performance of $PM_{2.5}$ also met the standards set by Huang et al. (2021),³¹ with R values for 2021 and 2022 ranging from 0.6 to 0.9 and NMB values ranging between -7 and 12%. Figure S2 shows the comparisons between simulated and observed PM_{2.5} chemical species, including SO₄²⁻, NO₃⁻, NH₄⁺, OC, and EC at the Dianshan Lake site, located in Shanghai. The model captures variations of these major components reasonably well in both years, with an R value ranging between 0.37 and 0.48.

Figure S3 illustrates the model performance on vertical temperature profiles (from the surface to 150 hPa). For 2021 and 2022, the R for the three provinces and one municipality exceeded 0.97, with NME and NMB below 2%. For PBLH (Figure S4), the R of the WRF–CMAQ simulation at the Shanghai Pudong site was 0.69 in both 2021 and 2022, with MB of 22.3 and 47 m and NMB of 3.4 and 7.2%, respectively. For the O₃ profiles (Figure S5), the R of the WRF–CMAQ simulation at the Shanghai Pudong site was 0.88 and 0.91 for 2021 and 2022, respectively. The MB were 9.3 and 6.4 ppb, with NMB of 13.6 and 13.1%, respectively. Figure S6 shows the simulation results of AOD. The model captured the characteristics of high AOD in the northern part and low AOD in the southern part of the YRD and successfully captured the significant reduction in aerosol in Shanghai and its surrounding

areas during the lockdown period (Maximum MB of -0.02), with R between 0.53 and 0.76. Figure S6 also shows the simulation results of HCHO/NO₂ column concentrations for WRF–CMAQ. The values in Shanghai from 2021 were mostly between 0.73 and 1.36, 18 reaching 1.68 in 2022, which our simulation accurately reproduces.

3. RESULTS

3.1. Changes in Air Pollutants and Meteorological Parameters. Figure 2d shows the variations in ground-level O₃, NO₂, and PM_{2.5} from surface observations, AOD from the Himawari-8 satellite, the ratio of HCHO/NO₂ column concentration from the Sentinel-5 satellite, and key meteorological parameters including RH, Tem, WS, and Pre from surface observations, as well as PBLH, SSR, and TCC from ERA5, during April to May 2022 relative to the same period in 2021.

Surface observations revealed a consistent increase in O₃ concentrations across the YRD region during April and May 2022 compared to 2021, with average increases of 10 ppb, 8 ppb, and 8 ppb observed in Shanghai, Jiangsu, and Anhui, respectively, and a relatively smaller increase (3 ppb) in Zhejiang (Figure 2a). The lockdown measures primarily affected anthropogenic emissions in Shanghai and southern Jiangsu. Satellite data indicated a 53-96% increase in HCHO/ NO₂ column concentrations (Figures 2b and S6a,b), suggesting a shift from a VOC-limited regime to a VOC-NOx co-limited regime, likely driven by the more significant reduction in NOx emissions compared to VOCs. Concurrently, PM_{2.5} concentrations decreased markedly (Figure 2a), with reductions in SO₄²⁻, NO₃⁻, NH₄⁺, OC, and EC at Dianshan Lake also decreasing by 30-60% overall. AOD also declined by 30-50% in Shanghai and southern Jiangsu (Figures 2a and S6c,d). These aerosol reductions may have enhanced radiation, potentially altering heterogeneous reactions and photolysis rates and thereby contributing to elevated levels of O₃.

In Shanghai and southern Jiangsu, the impact of meteorological changes on the O₃ variations is complicated: SSR increased, while Tem and RH decreased (Figures 2c and S1a-c). Meanwhile, HCHO/NO₂ ratios rose by 40–50% in northwestern YRD (Anhui and northern Jiangsu, Figure S6a,b). Since the lockdown had a minimal direct impact on these areas, the HCHO/NO₂ increase is primarily attributed to meteorological changes. Notably, the entire northwestern YRD experienced significant rises in Tem and SSR, coupled with substantial RH decreases (Figures 2c and S1a,c), indicating that 2022 meteorological conditions were particularly con-

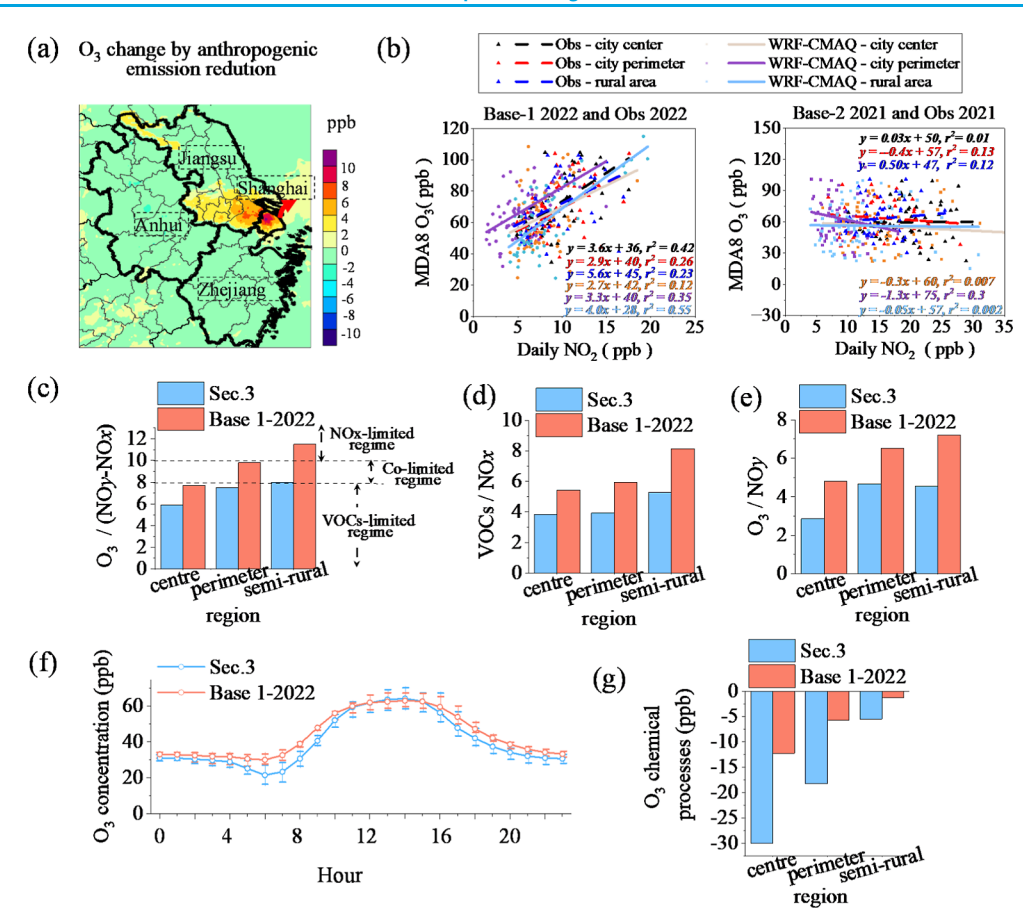


Figure 4. Changes in concentrations of O_3 and its precursors caused by anthropogenic emission reduction. (a) regional distribution of O_3 concentration changes due to emission reduction in the YRD. (b) the MDA8 O_3 /daily NO_2 concentration in surface observation and WRF–CMAQ in different areas of Shanghai. (c–e) O_3 /(NO_2 - NO_2), VOCs (ppbC)/ NO_2 , and O_3 / NO_2 in different areas of Shanghai from WRF–CMAQ. (f) diurnal O_3 variation between Base 1-2022 and Sce.3-2022M2021A scenarios in Shanghai. (g) surface O_3 chemical processes variation between Base 1-2022 and Sce.3-2022M2021A scenarios.

ducive to O_3 formation in this region. In contrast, the variation of the levels of O_3 in Zhejiang (3 ppb) was relatively minor compared to other regions; while the results for Zhejiang are retained in subsequent discussions, they are not analyzed comprehensively.

Based on these observed changes in meteorology and air pollutants, we preliminarily identified the year-on-year changes in meteorological conditions and anthropogenic emissions in the YRD region during April to May 2022. For Shanghai and southern Jiangsu, lockdown-driven emission reductions led to a shift in O_3 -limited regimes, resulting in increased O_3 concentrations. Aerosol concentrations also changed significantly in these areas, although their impact on O_3 requires further investigation. The increase in the level of O_3 in the northwestern YRD, rarely affected by lockdown measures, is attributed to the more favorable 2022 meteorological conditions for the formation of O_3 . While the above discussion is qualitative, further quantitative analysis is necessary to confirm the relative contributions of varied factors to the observed O_3 changes.

3.2. Impacts of Meteorological Changes on O_3 Variations. To quantitatively assess the influence of meteorological conditions on the O_3 fluctuations, we conducted WRF-CMAQ modeling runs for the YRD in 2022 under a baseline scenario (base 1-2022) and a parallel scenario identical to the Base case but incorporating the 2021 meteorological fields (Sec.1-2021M2022E). The results

(Figure 3a) indicated that meteorological changes contributed to an overall variation in the level of O_3 of 5 ± 3 ppb in the northwestern YRD, -4 ± 1 ppb in Shanghai, 0 ± 2 ppb in southern Jiangsu, and -3 ± 2.5 ppb in Zhejiang. The increase in the level of O₃ in northwestern YRD due to meteorological changes was anticipated, as observations show that the air was drier and the SSR was stronger in 2022, creating an atmospheric environment more conducive to O₃ formation. Conversely, the 2022 meteorological conditions had a significantly negative impact on the level of O₃ in Shanghai compared to 2021. Since observational data alone is insufficient to determine the impact of meteorological factors on O₃, we conducted PA to further investigate the reasons behind this negative contribution (the PA results discussed here include both horizontal and vertical advection and diffusion processes across the whole Shanghai domain). As shown in Figure 3b, PA results indicated that, compared to 2021, the 2022 meteorological conditions enhanced O₃ photochemical production in Shanghai, consistent with the increased photolysis rates of surface NO2 and other precursors observed by Zhu et al. (2023). 18 As shown in Figure 3c, the diffusion in 2022 near the surface decreased significantly, with values reaching up to -3 ppb, whereas the changes in diffusion just above the surface were minor. This vertical pattern indicated that the reduction in surface O₃ was primarily caused by substantially weakened downward transport from upper layers, rather than by enhanced upward mixing of near-surface

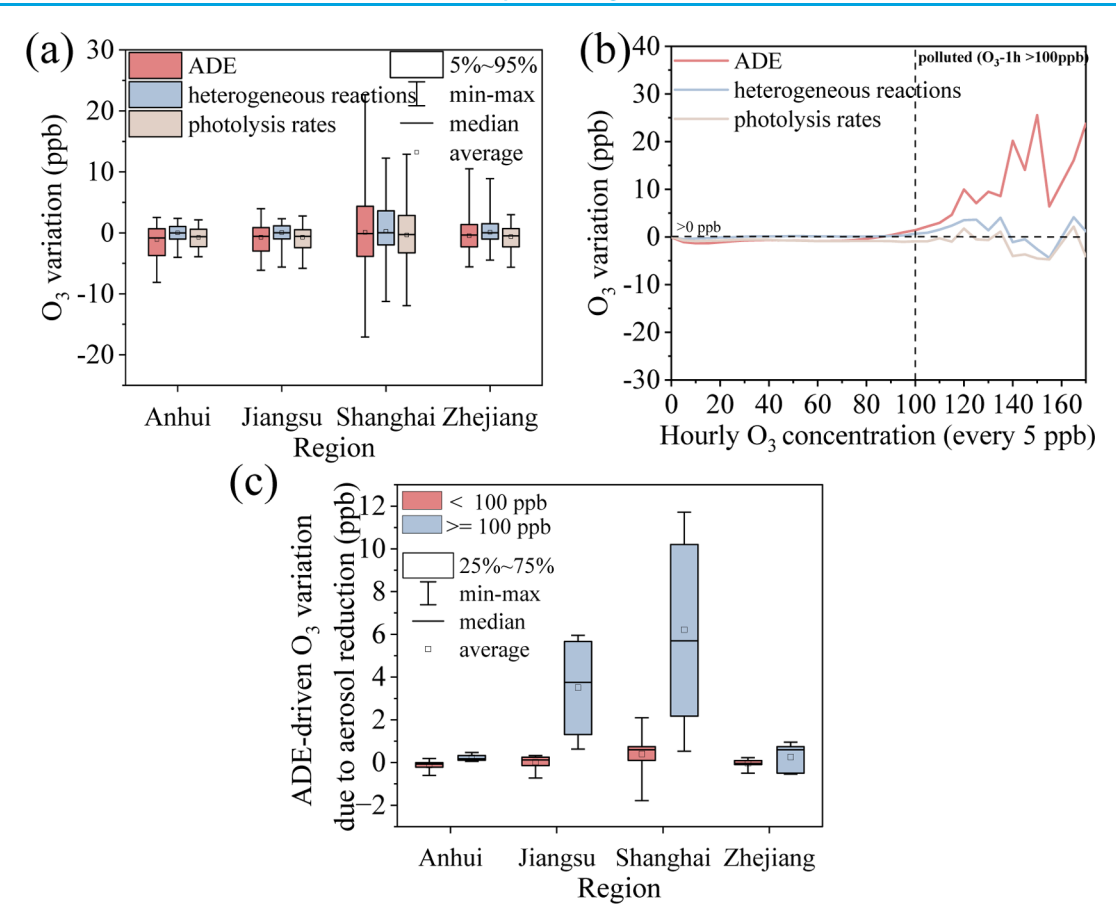


Figure 5. Effects of ADE, heterogeneous reaction, and photolysis rates on hourly O_3 . (a) contribution of three effects to O_3 concentration in the YRD region (hourly time resolution), while (b) impact of the three effects on O_3 based on the concentration of O_3 . (c) O_3 variation due to ADE by aerosol reduction.

 O_3 . Additionally, advection under 2022 meteorological conditions contributed to a further decrease of 1 ppb, suggesting reduced O_3 transport (consistent with the cleaner wind directions reported by Tan & Wang (2022)¹⁵) and enhanced removal processes. This also implies that the increased O_3 concentration in the northwest YRD had a negligible impact on Shanghai.

Differences in biogenic emissions between the two adjacent years were almost entirely meteorology-induced. Therefore, the impact of changes in biogenic VOC emissions is an indirect effect of meteorological factors. Figure S7 shows that the variation in mean $\rm O_3$ concentrations due to differences in biogenic VOC emissions in 2022 (difference between Sce.2-2022M2021B and Base 1-2022) was insignificant compared with the direct effects of anthropogenic source precursors and meteorology. The level of $\rm O_3$ in Shanghai increased by 0.6 \pm 0.1 ppb, while other provinces experienced changes ranging between -0.1 and 0.4 ppb due to BVOC emission changes driven by meteorological variations.

Overall, the more favorable meteorological conditions for the photochemical production of O_3 in 2022 primarily drove the increase in O_3 of O_3 in the northwestern YRD, with a maximum rise of 6 ppb. Meanwhile, although meteorological conditions were favorable for surface O_3 photochemical production in Shanghai, a reduced diffusion contribution and enhanced atmospheric removal resulted in an overall contribution of -4 ppb.

3.3. Impacts of Anthropogenic Emission Changes on

O₃ Variations. The emission reductions caused by the COVID-19 lockdown in Shanghai in 2022 were primarily concentrated in Shanghai and southern Jiangsu. In Shanghai, emissions of NOx, VOCs, and PM decreased by 50%, 40%, and 70%, respectively; in Jiangsu, NOx, VOCs, and PM emissions were reduced by 37%, 25%, and 40%, respectively. Overall, the lockdown resulted in higher reductions in NOxcompared to VOCs, as confirmed by the observed changes in HCHO/NO₂ column concentrations. WRF-CMAQ modeling results (difference between Sce.3-2022M2021A and Base 1-2022) indicated a significant increase in O₃ concentrations in Shanghai and its adjacent areas due to the reduction in anthropogenic precursor emissions (Figure 4a). The most pronounced O3 changes were observed in Shanghai and southern Jiangsu, with O_3 increasing by 9 ± 1 ppb and 5 ± 2 ppb, respectively. This increase is attributed to imbalanced precursor emission reductions.

Specific indicators are often used to characterize the O_3 chemical regime. Figure 4b shows the ratios of the mean maximum daily 8 h average O_3 concentrations (MDA8 O_3) to daily NO_2 concentrations from WRF–CMAQ simulations and ground observations across different regions of Shanghai (for site locations, refer to Tan & Wang $(2022)^{15}$). Both observed and model results indicated that the MDA8 O_3/NO_2 slope in the city center area is lower than in rural areas, which aligns with the characteristic that O_3 in the city center area is more sensitive to VOCs due to high NOx emission from vehicle

exhaust. In 2021, the MDA8 O₃/daily NO₂ slopes derived from observations ranged from -0.4 to 0.5 ppb ppb⁻¹ (across different urban areas), while the Base 1-2021 simulated slopes ranged from -1.3 to -0.05 ppb ppb⁻¹ (Figure 4b, right). In 2022, observational slopes increased markedly to 2.9-5.6 ppb ppb⁻¹, and the Base 1-2022 simulated slopes showed a comparable range of 2.7–4.0 ppb ppb⁻¹ (Figure 4b). These results demonstrate a clear shift trend in the O₃-NO₂ relationship, indicating that the O₃ photochemical regime in 2022 was much more VOC-limited than in 2021. Figure S6a,b,e,f illustrates the HCHO/NO₂ column concentration ratios derived from WRF-CMAQ simulations and satellite observations. In 2022, concentrations increased by approximately 50% in Shanghai, its surrounding areas, and along the Yangtze River shipping lanes (a primary NOx emission source from vessels), indicating a higher relative abundance of HCHO compared to that of NO₂. Figure 4c shows the O₃/(NOy-NOx) ratios across different regions and scenarios in the WRF-CMAQ simulations. Compared to city perimeter areas and rural areas, the city center area exhibited lower $O_3/(NOy-$ NOx) values. Under the Sce.3-2022M2021A scenario, both city center area and perimeter areas remained within a VOClimited regime (<8, following Sillman and He (2002)³³ and Li et al. (2011)³⁴). However, emission reduction in the Base 1-2022 scenario shifted central urban sites closer to a VOC-NOxcolimited regime, city perimeter areas into the colimited regime (8-10), and rural area into a NOx limited regime (>10). Similarly, the level of O_3 (NOy-NOx) values in areas surrounding Shanghai also increased (Figure S8). Figure 4d,e illustrate changes in VOCs/NOx and O₃/NOy concentrations from WRF-CMAQ output, both of which confirm that O₃ sensitivity to NOx increased in 2022.

We also tracked the diurnal changes of the O_3 concentration under two scenarios. Figure 4f presents the diurnal variations of O_3 for both scenarios, showing that reduced NOx emissions led to increased nighttime O_3 concentrations, while daytime peak concentrations decreased. Additionally, the peak shape became broader and more prolonged, which is a typical characteristic of the transition from a VOC-limited regime to a NOx-VOC co-limited or even a NOx-limited regime. Figure 4g illustrates the surface O_3 chemical processes concentration derived from PA. Under the lockdown measures in Shanghai, the O_3 loss due to NO titration decreased by $70 \pm 10\%$, further indicating NO deficiency.

Overall, surface observations, satellite measurements, and WRF–CMAQ simulations of precursor and O_3 concentration changes consistently indicated that the greater reduction in NOx compared to VOCs due to lockdown measures led to a significant increase in O_3 concentrations in Shanghai and surrounding VOC-limited regime area, shifting the O_3 control regime toward the NOx-limited regime.

3.4. Impact of Aerosol on O_3 via ADE, Photolysis, and Heterogeneous Reactions. Aerosols can cool the surface atmosphere through ADE and influence O_3 by affecting heterogeneous reactions and photolysis rates. Here, we first focus on the effects of ADE, heterogeneous reaction, and photolysis rate on O_3 in the YRD region, excluding the effects of aerosol emission reduction because aerosol effects on O_3 are indirect and differ significantly from meteorological factors and precursors. As shown in Figure S_3 , the impacts of these three effects on monthly average O_3 concentrations are relatively small, ranging within ± 1 ppb. However, their maximum impact on hourly O_3 concentrations can reach 3-25 ppb in different

areas, indicating the potential for aerosols to affect hourly O₃ concentrations. Further analysis revealed that their influence becomes notably higher when the O₃ concentrations are higher than 90–100 ppb (Figure 5b). In the following analysis, we use 100 ppb as a threshold, as it corresponds to the hourly O₃ concentration standard in China. Within the range of hourly O₃ concentrations higher than 100 ppb, the average impact of ADE was 10.8 ppb. Furthermore, ADE increased pollution days (MDA8 O₃ > 80 ppb) by an average of 2% across all monitoring sites in Shanghai, 2% in Anhui, 1% in Jiangsu, and 0.3% in Zhejiang (Figure S9). In contrast, the other two effects did not influence the occurrence of pollution days, highlighting that ADE's impact on O₃ pollution is more significant. Notably, when O₃ concentrations were high, ADE's impact on average O₃ concentration across the YRD (Figure 5b) and in the three provinces and Shanghai (Figure S10) was almost entirely positive, contrasting with the other two effects, which showed both positive and negative impacts.

Compared to 2021 emissions, the 2022 emission background altered the monthly average O3 concentration in Shanghai, Jiangsu, Anhui, and Zhejiang by 0.6 ± 0.2 , 0.1 ± 0.4 , -0.05 ± 0.1 , and -0.1 ± 0.1 ppb, respectively. The impact on the monthly average concentration was small, but from a diurnal perspective (Figure S11), changes in Shanghai and Jiangsu were between 0.54-1.65 ppb and 0.21-0.67 ppb, respectively, which were higher than the monthly averages and higher than those in the other provinces. Furthermore, within hourly O₃ concentrations higher than 100 ppb, ADE led to O₃ changes in Shanghai and Jiangsu by 6.2 ppb (0.5–12 ppb) and 3.5 ppb (0.6-6 ppb), respectively (Figure 5c), due to the emission variations, with a significant increase in the level of impact compared to non-pollution days. The greater impact of emission changes in Shanghai and Jiangsu compared to other provinces was reasonable, as the extent of emission change in Anhui and Zhejiang was significantly smaller. The effect of emission changes on heterogeneous reactions and photolysis rates was relatively weak during this period and will not be discussed in detail here.

In summary, ADE exerts a relatively greater impact on high O₃ concentration (>100 ppb), with an average increase of 10.8 ppb. Previous studies have similarly reported the influences of ADE on hourly O_3 levels. For instance, Xing et al. $(2017)^{36}$ used WRF-CMAQ simulations to show that ADE could increase monthly mean maximum peak 1 h O_3 by up to 4 μg m $^{-3}$ in July. Zhao et al. $(2023)^{39}$ also found that ADE led to a monthly average increase of 4 μ g m⁻³ in O₃ concentrations over the Beijing-Tianjin-Hebei region. In this study, lockdown-related emission changes contributed to ADE-driven increases in high O₃ concentrations (>100 ppb), with rises of 6.2 ppb (0.5-12 ppb) in Shanghai and 3.5 ppb (0.6-6 ppb) in Jiangsu, respectively. Similarly, Wang et al. (2016)³⁷ reported that reducing aerosol emissions increased surface O₃ by up to 3.6 ppb in eastern China, supporting the enhancing effect of aerosol reductions on O3 increase. Our results highlight that large-scale aerosol reductions have a noteworthy impact on the level of O₃, providing a supplementary perspective for this YRD case. However, the detailed mechanism by which ADE influences the level of O₃ remains unclear and requires further analysis.

3.5. Mechanism of the ADE Effect on O_3 . Our analysis revealed that ADE has a more pronounced impact during high O_3 concentration periods, positively influencing the average O_3 concentration in Shanghai and negatively in other regions.

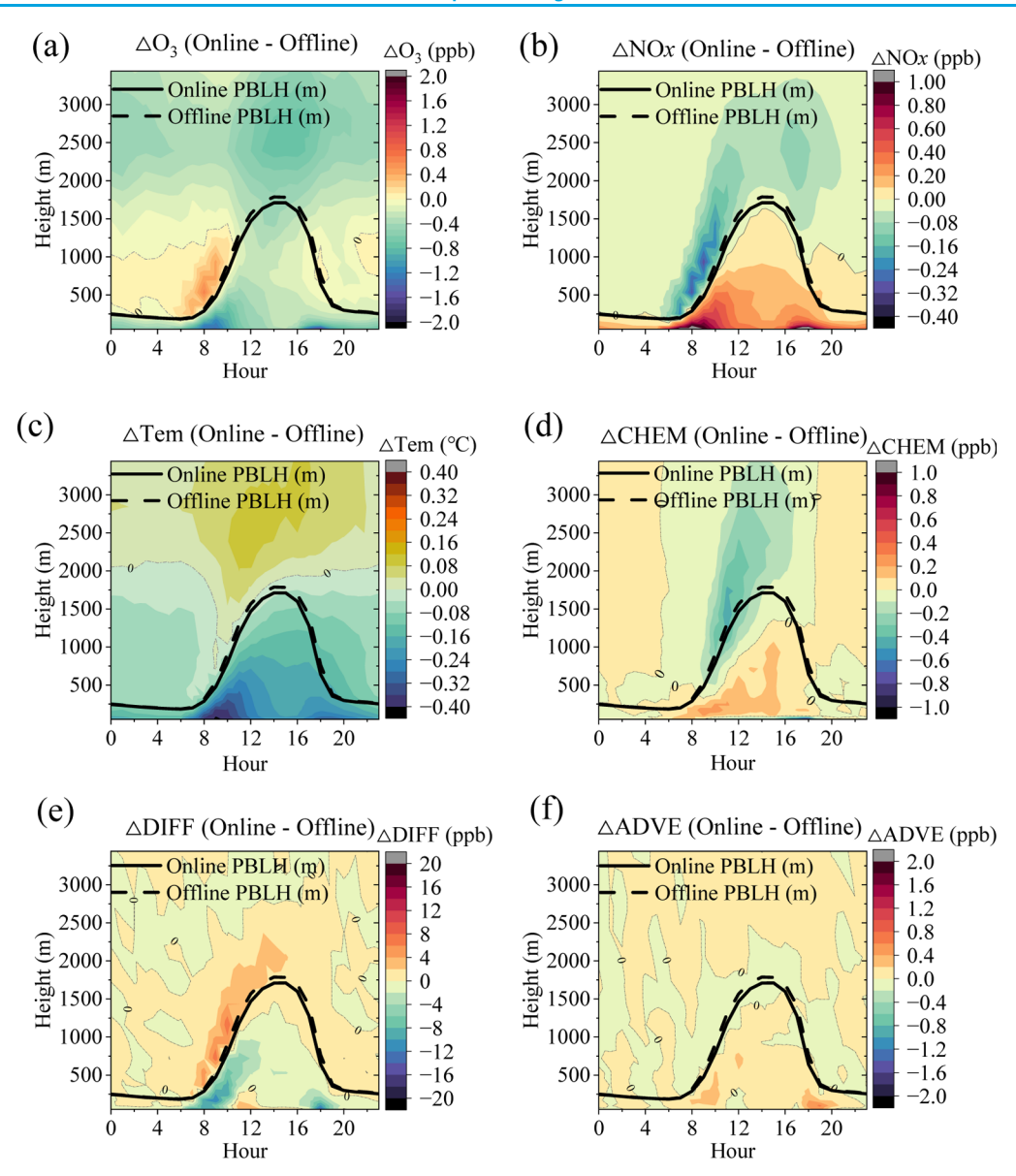


Figure 6. Averaged diurnal difference between online and offline O_3 concentration (a), NOx concentration (b), Tem (c), chemical processes (d), diffusion processes (e), and advective processes (f) and boundary layer height diurnal differences from the surface to high altitude (0–3440 m) over the entire YRD domain. Chemical processes, advection processes, and diffusion processes were labeled CHEM, ADVE, and DIFF in the figure, respectively.

Additionally, aerosol emission reductions led to an increase in the concentration of O_3 concentrations. To further explore the mechanism of ADE on O_3 , we compared the results of Base 1-2022 (hereafter referred to as the "online scenario") and Sce.4-ADE a (offline scenario).

Between 6:00 and 7:00, O₃ concentrations in the online scenario were higher above the boundary layer but lower below it compared to the offline scenario (Figure 6a), while NOx concentrations exhibited the opposite trend (Figure 6b). During this period, the O₃ photochemical reactions were not yet active, and the differences were mainly attributed to atmospheric physical processes. In the early morning, surface heating and the dissipation of the nocturnal inversion layer led to significant vertical diffusion (evidence from ERAS and model-predicted vertical temperature vertical profile changes is shown in Figures S12 and S13). Surface O₃ primarily originates from upper nighttime residuals (Figure S14a), and the replenishment of high-altitude NOx depends on surface

emissions, particularly vehicle exhaust during traffic peaks. This indicated that ADE hinders vertical atmospheric movement, causing more O_3 to accumulate above the boundary layer and NOx to accumulate below it. This hindering effect is due to ADE slowing down surface heating (Figure 6c) and reducing the vertical temperature gradient. Interestingly, Langenbrunner et al. (2017), 40 based on the WRF model, reported that CO_2 enhanced surface temperatures, weakened atmospheric stability, and reduced Amazonian precipitation. In this study, ADE reduces surface temperatures, strengthening atmospheric stability and weakening vertical atmospheric movement.

From 8:00 to 12:00, ADE gradually reverses the trend of surface O_3 concentration decrease observed between 6:00 and 7:00. This is due to two main factors. First, the increase in the SSR enhances photochemical reactivity (Figure S14b). With more NO α accumulated below the boundary layer, photochemical reactions in the upper levels of the boundary layer are

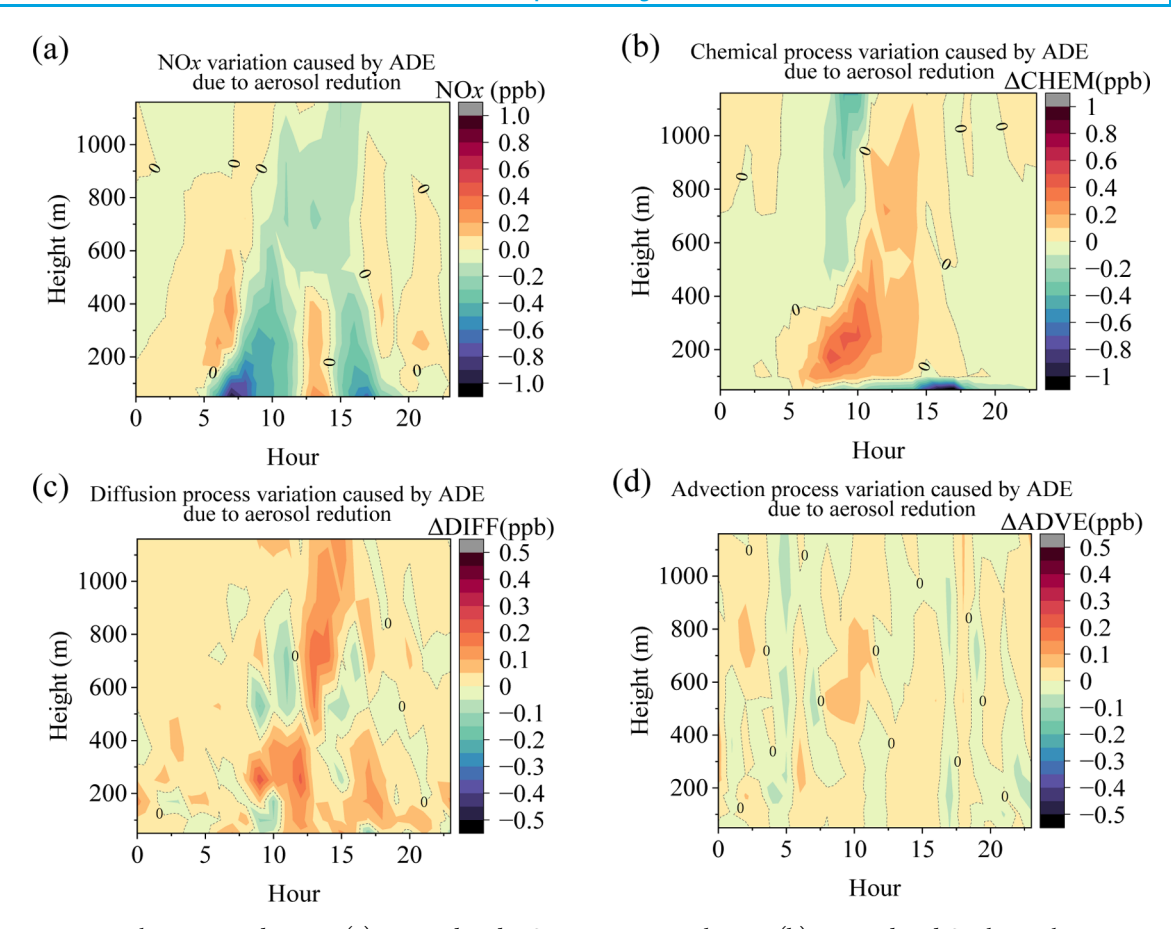


Figure 7. Due to aerosol emission reductions, (a) ADE-induced NOx concentration changes, (b) ADE-induced O $_3$ chemical process concentration changes, (c) ADE-induced O $_3$ diffusion process concentration changes, and (d) ADE-induced O $_3$ advection process concentration changes in Shanghai and Jiangsu. Chemical processes, advection processes, and diffusion processes were labeled CHEM, ADVE, and DIFF in the figure, respectively.

strengthened (Figure 6d), leading to increased concentrations of O₃ from the high-altitude atmosphere to the surface through diffusion (Figure 6e). Second, as the temperature rises, the boundary layer gradually lifts, facilitating the mixing of O₃ between the high-altitude and surface. The O₃ that had accumulated above the boundary layer at 6:00-7:00 is then diffused to the surface, further increasing the concentration of O₃ from the high altitude to the surface by diffusion (Figure 6e). After 12:00, although high-altitude O₃ photochemical contributions below the boundary layer in the online scenario remain more active than those in the offline scenario, the decrease in the O₃ gradient between the surface and highaltitude (Figure S14a) and the consumption of nighttime O₃ above the boundary layer led to a significant reduction in diffusion (Figure S14c). Consequently, the influence of ADE on diffusion weakens (Figure 6e), and the positive trend of surface O₃ gradually flattens (Figure 6a). Between 16:00 and 18:00, photochemical reactions weaken, and NOx emissions significantly increase again (during the rush hour). Like the situation at 6:00-7:00, ADE continues to cause NOxaccumulation below the boundary layer (Figure 6b), leading to more pronounced NO titration in the online scenario (Figure 6d), and the concentrations of O₃ drop again (Figure 6a). After 18:00, SSR gradually diminishes, and ADE effects diminish as well, with all differences tending toward their minimum values. When considering the ADE-induced O₃ changes averaged over the diurnal, advection plays a relatively minor role compared to diffusion (Figures 6f and S14d).

Summarizing the mechanism of ADE in this YRD case, a key point is that it leads to an increase in NOx concentration below the boundary layer near 6:00-7:00, which further induces an increase in the photochemical contribution of highaltitude O₃ from 8:00 to 15:00. This explains why ADE has a greater impact on Shanghai. Previous studies have shown that although Shanghai is in the VOCs or VOCs-NOx co-limited regime, during periods of intense photochemical reactions in the morning and noon, NOx is rapidly consumed due to its extensive participation in O₃ photochemical processes. As a result, Shanghai's sensitivity to NOx is significantly higher than to VOCs from 8:00 to 15:00. 41,42 And it is also higher than that of other provinces in the YRD. The sensitivity of O₃ in Shanghai to NOx is further enhanced due to the higher reduction ratio of NOx emissions than VOCs caused by the lockdown measures. In fact, due to the lockdown, NOxemissions in Shanghai decreased substantially, resulting in a lower increase in NOx in the early morning (0.45 \pm 0.4 ppb) compared to that in other provinces $(0.73 \pm 0.6 \text{ ppb})$ caused by ADE. However, the chemical processes contributing to the level of O_3 in Shanghai (5.8 \pm 5.3 ppb) were higher than in other provinces $(3.5 \pm 2 \text{ ppb})$ below the boundary layer.

Another key factor influencing ADE's impact on O_3 is meteorological conditions. Based on the preceding discussion, we hypothesize that ADE is more likely to exert a positive effect on the level of O_3 when atmospheric conditions are favorable for photochemical production and vertical mixing. To test this hypothesis, we further investigated the relationship

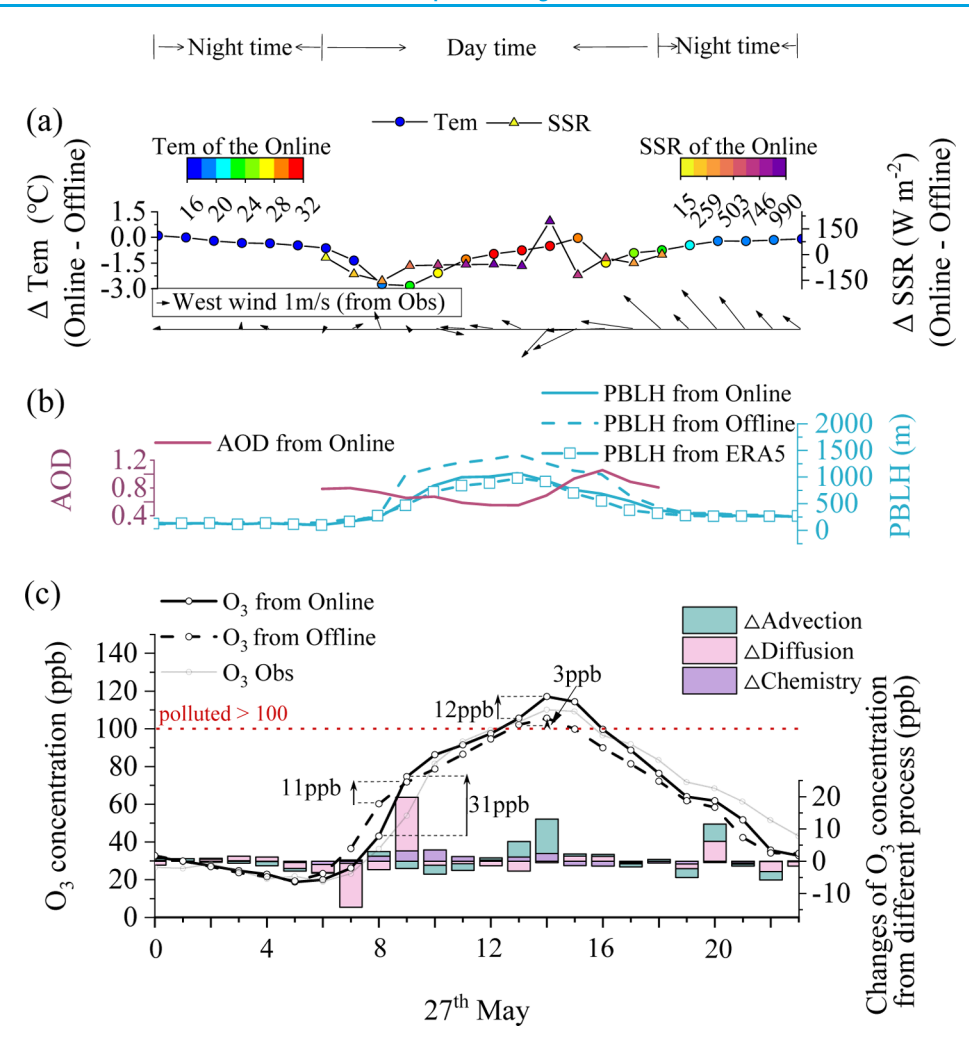


Figure 8. Contribution of ADE to O_3 pollution on May 27th in Shanghai. (a) Two top dots lines represent Tem and SSR from WRF–CMAQ, respectively, and the color represents their values. The wind vector represents the WS and WD of Shanghai urban area from observation. (b) The line with dot represents observational PBLH, the solid line represents the PBLH from Online scenario, and the dashed line represents the PBLH from Offline scenario, (c) The black dotted line in the figure represents the O_3 concentration in the Online scenario, the dotted line represents the Offline scenario, the gray dotted line represents observation, and the bar chart represents the contribution of different physical and chemical processes to O_3 .

among ADE-induced changes in the level of O₃ and PBLH, RH, and Tem. Figure S15a illustrates the association between the PBLH growth rate (from 08:00 to 12:00, across various stations and days) and the ADE-induced change in surface O₃ concentration. It is evident that when the PBLH growth rate exceeds 200 m/h, the average increase in the level of O₃ attributable to ADE rises markedly—from approximately 0 to nearly 1 ppb. Overall, ADE's influence on surface O₃ exhibits a positive correlation with the PBLH growth rate, underscoring the importance of vertical transport in enhancing ADE effects. Figure S15b illustrates the relationship between ADE-induced changes in the concentration of O₃ within the boundary layer above 100 m (from 08:00 to 12:00, across various stations and days) and both RH and Tem. As anticipated, under drier and warmer conditions (RH < 40%, Tem >15 °C), photochemical activity is enhanced, and ADE tends to cause greater increases in O₃ concentrations. When RH is higher, it typically indicated less favorable conditions for O_3 formation 43,44 and reduced PBLH growth rates, 45,46 consequently leading to decreased ADE-driven O₃ concentration changes. However, it is noteworthy that even under higher RH conditions, ADE still retains the potential to increase the level of O_3 concentrations,

primarily through transport processes. These data explain why ADE has a greater effect on O_3 at higher surface O_3 concentrations: favorable high-altitude photochemistry and active vertical mixing often coincide with high surface O_3 . In summary, while the average impact of ADE on surface O_3 in the YRD during April to May is relatively modest, under specific meteorological and regional conditions, ADE has the potential to significantly enhance O_3 pollution.

One remaining question is why the ADE-driven increase of O₃ O₃ increase in O₃ in Shanghai and Jiangsu under lower aerosol concentrations and lower O₃ precursor concentrations exceed that under higher aerosol and higher O₃ precursor concentrations? This can be attributed to the coupled effect of ADE and the shifting of the O₃ control regime. Figure 7a shows that under higher aerosol and O₃ precursor concentrations, ADE-induced increases in NOx concentrations are significantly higher compared to lower aerosol and O₃ precursor concentrations. One reason is the previously confirmed reduction in the NOx concentrations. In addition, Figure S16 shows the diurnal variations of major PM_{2.5} components most relevant to the ADE effect—SO₄²⁻, NO₃⁻, OC, NH₄⁺, and EC⁴⁷—all of which exhibited lower

concentrations in 2022 compared to 2021, indicating an overall weakening of the ADE in 2022. However, given the 2022 emission background, Shanghai and Jiangsu exhibited a greater sensitivity to NOx. Consequently, the enhancement of highaltitude O_3 photochemistry was enhanced $(0.6 \pm 0.2 \text{ ppb})$ under the 2022 emissions scenario (Figure 7b). This enhancement further led to stronger downward diffusion (Figure 7c) and eventually higher surface O₃ concentrations (Figure S10), while advection played a relatively minor role in the diurnal mean ADE-induced O₃ changes (Figure 7d), as previously discussed in the ADE effect mechanism. This is the fundamental reason ADE-driven O3 increases were higher under the 2022 emission background compared to the 2021 emission background. It should be noted that the magnitude of the ADE is sensitive to aerosol chemical composition: scattering species such as $SO_4^{\,2-}$ and $NO_3^{\,-}$ primarily cool the atmosphere by attenuating incoming solar radiation, whereas absorbing components—especially black carbon and brown carbon—warm the boundary layer and can enhance vertical mixing. $^{48-50}$ Therefore, reductions in different aerosol components may lead to opposing changes in the ADE intensity. However, given the substantial overall decline in aerosol concentrations and the significant reduction in major scattering components such as SO_4^{2-} and NO_3^{-} , which account for a large fraction of PM_{2.5} (Figure S16), a weakened ADE in 2022 is reasonable and expected. Due to the constraints of the current model configuration, our study represented aerosols using bulk optical properties and therefore does not resolve the composition-specific contributions to ADE.

3.6. Case Study on the Impact of ADE on O₃. To deepen our understanding of the ADE effect on O₃, we compared online and offline scenarios during a typical O₃ pollution episode. We screened an O₃ pollution case in Shanghai on May 27th, 2022, with an MDA8 O₃ of 92 ppb and nighttime concentrations reaching 60 ppb at 20:00 (Figure 8). Figure 8a shows a strong easterly wind occurring in the afternoon, indicating the influence of regional transport. For this day's O₃ simulation, the *R* value was 0.97, MB was 3.98 ppb, and NMB and NME were 7 and 10%, respectively. Figure 8b also shows the model's performance in simulating PBLH compared to ERA5 data, with an *R* of 0.99 and NMB of 14%. These results indicated that the simulations were robust enough to be used for further analysis.

Between 6:00 and 7:00, reduced diffusion in the online scenario led to lower surface O₃ concentrations compared with the offline scenario. After 8:00, surface O₃ concentrations in the online scenario exceeded those in the offline scenario (Figures 8c and S17). As previously discussed, increased highaltitude O₃ production (Figure S18) and downward transport of retained O₃ at high altitude caused a rapid increase in surface O₃ in the online scenario (maximum to 31 ppb), much higher than in the offline scenario (maximum to 11 ppb). Contrary to expectations, the O₃ concentration difference between the two scenarios did not level off from 12:00 to 14:00. Instead, the online scenario showed a notable increase, 9 ppb, higher than the offline scenario. Further analysis revealed that this change was related to the regional transport. During this period, differences in advection and enhanced easterly winds indicated a clear regional transport of an O₃ pollution plume (Figure 8). The online scenario had more O₃ advection transport, leading to a more significant increase in surface O_3 concentration. The source of this pollution plume

was located off the coast near the Yangtze River estuary northeast of Shanghai (Figure S19, purple circle). Starting from 11:00, a wind convergence zone gradually formed in this area, causing O₃ to accumulate and forming an O₃ pollution plume. In the online scenario, the concentrations of O_3 in the wind convergence zone were 10-25 ppb higher than in the offline scenario (Figure S19). Due to the lack of NOx emission sources over the ocean, and contrary to previous descriptions, ADE cooling led to a lower chemical contribution of highaltitude O_3 in the online scenario in this area (Figure S20a,b). More O₃ transport (diffusion plus advection) accounted for the higher surface O₃ concentrations in the wind convergence zone of the online scenario (Figure S16c,d). The logical inference is that ADE results in higher high-altitude O₃ concentrations in inland Shanghai in the morning, causing the wind convergence zone to entrain more O₃ from inland Shanghai (west direction wind in Figure S19), thus increasing surface O_3 concentrations in the online scenario. Eventually, the higher O₃ concentration reached inland Shanghai with the strengthened easterly winds, leading to an increase in the level of O_3 and an overnight high-value O_3 event.

In addition to examining the differences between the online and offline scenarios, we further incorporated the effects of emission reductions into the analysis. Figure S21 supplements the case analysis by illustrating the ADE-induced changes in the level of O₃ resulting from emission reductions. Consistent with the process discussed in Section 3.5, due to the substantial reduction in NO emissions, the surface NO concentrations within the boundary layer under the 2022 emissions scenario in the morning were only 30-50% of those under the 2021 emission scenario, and the ADE-induced increase in NO was also lower (Figure S21a). However, due to higher NO sensitivity under the 2022 emission background, ADE led to greater O₃ chemical production (Figure S21b) below the boundary layer, resulting in a larger ADE-induced surface O₃ increase (0.7 ± 0.5 ppb, Figure S21c). Under the 2021 emission background, the higher NO concentrations made a more pronounced positive contribution to the formation of the surface O₃ during midday, when photochemical reactions were strongest. As a result, the rate of the increase in the level of O₃ was faster, and the concentration of O₃ eventually slightly exceeded that under the 2022 emission background. Meanwhile, due to reduced radiation in the evening, the higher NO emissions also led to a faster decline in the concentration of O₃ (Figure S21c).

In summary, this case has two important implications: first, the influence of ADE can be regionally transmitted through atmospheric physical processes. Second, special weather conditions, such as wind convergence, may amplify the impact of ADE.

4. DISCUSSION

In this study, we combined observational data and the online WRF–CMAQ model to quantitatively analyze the driving factors behind the increase in O_3 concentrations in the YRD region during Shanghai COVID-19 lockdown from April to May 2022 and mechanisms of ADE on O_3 . 10% higher reduction in NOx relative to VOCs led to an O_3 increase of 9 \pm 1 ppb in Shanghai and 5 \pm 2 ppb in southern Jiangsu. Meteorological changes caused O_3 variations of 5 \pm 3 ppb in northwestern YRD, -4 ± 1 ppb in Shanghai, and 0 \pm 2 ppb in southern Jiangsu. Due to emission reductions, ADE increased O_3 concentrations (O_3 -1h > 100 ppb) by 6.2 and 3.5 ppb in

Shanghai and Jiangsu, respectively. The rise of the level of O₃ in Anhui and northern Jiangsu was almost entirely due to meteorological changes, while increases in Shanghai and southern Jiangsu are attributable to combining precursor emission reductions, meteorological changes, and aerosol emission reductions. Our results explain 65-85% of the observed O₃ increase in Shanghai, Jiangsu, and Anhui, with the remaining unexplained primarily attributed to model uncertainties. These findings suggested that, in urban areas that are primarily VOC-limited regime, an inappropriate NOx/ VOCs reduction ratio could lead to an increase in O₃ concentrations. This real-world case during the COVID-19 lockdown emphasizes the importance of selecting appropriate NOx/VOCs emission reduction strategies. Notably, spring temperature fluctuations of 1.0-2.5 °C can induce 10-15% O₃ variations across the YRD. CMIP6 projects a 1-3 °C warming over the next 20 years,⁵¹ suggesting an increased risk of exacerbated springtime O₃ pollution in the future. Mitigating this climate impact will require further precursor emission reductions. Moreover, meteorological factors influence not only O3 photochemical conditions but also its transport and removal. Inferring meteorological impacts on O₃ solely on the basis of average changes may be inaccurate, amplifying uncertainties in future O₃ management.

Previous studies regarding the impact of ADE on the level of O₃ have primarily focused on its average effects, lacking detailed descriptions of the underlying mechanisms. In this COVID-19 lockdown case, ADE resulted in an average increase of 10.8 ppb in O₃ concentrations above 100 ppb in the YRD region. Our analysis revealed that ADE cools the surface and suppresses atmospheric mixing early in the morning (06:00-07:00), causing O_3 accumulation above the boundary layer and increased NOx below the boundary layer. From 08:00 to 12:00, in VOC-limited regions, enhanced radiation and increased NOx concentrations amplify O₃ photochemical production, with the extent of enhancement depending on regional NOx sensitivity, thereby further increasing surface O₃ concentrations. Furthermore, as the temperature rises, boundary layer development facilitates the transport of O₃ retained at high-altitude from the upper boundary layer to the surface, leading to a further increase in surface O₃ concentrations. However, due to the relatively small impact of ADE on average concentrations (due to the counteracting effects of positive and negative influences), ADE is often overlooked. We also found through a case analysis that ADE could have cross-regional impacts. Diffusion, NOx emissions, the O_3 chemical regime, and weather conditions are key factors influencing the ADE effect. Although our study focuses on the spring season in the YRD, the framework of ADE impact mechanisms is applicable to other regions of the world and different seasons. Future studies should couple observations with explainable machine-learning frameworks to resolve the dynamics of the O₃ complex in full three-dimensional space. In particular, quantifying how individual aerosol species, via their distinct optical properties, amplify or offset the ADE, and how the aerosol indirect effect may further modulate this interplay.

ASSOCIATED CONTENT

Supporting Information

The Supporting Information is available free of charge at https://pubs.acs.org/doi/10.1021/acsestair.5c00130.

Additional experimental and modeling details, including quality assurance and quality control of observational data; estimation of emissions; model validation for meteorological parameters, O_3 , and $PM_{2.5}$ chemical species; ADE analysis on O_3 concentrations and pollution episodes; scenario comparisons between different emission and simulation settings; and vertical profile and diurnal variation analysis (PDF)

AUTHOR INFORMATION

Corresponding Author

Li Li – Key Laboratory of Organic Compound Pollution Control Engineering (MOE), School of Environmental and Chemical Engineering, Shanghai University, Shanghai 200444, China; orcid.org/0000-0001-5575-0894; Email: lily@shu.edu.cn

Authors

Zhixu Sun – Key Laboratory of Organic Compound Pollution Control Engineering (MOE), School of Environmental and Chemical Engineering, Shanghai University, Shanghai 200444, China

Jiani Tan – Key Laboratory of Organic Compound Pollution Control Engineering (MOE), School of Environmental and Chemical Engineering, Shanghai University, Shanghai 200444, China

Murnira Othman – Institute for Environment and Development (LESTARI), Universiti Kebangsaan Malaysia, Bangi, Selangor 43600, Malaysia

Yangjun Wang – Key Laboratory of Organic Compound Pollution Control Engineering (MOE), School of Environmental and Chemical Engineering, Shanghai University, Shanghai 200444, China

Juntao Huo – Shanghai Environmental Monitoring Centre, Shanghai 200235, China

Maggie Chel Gee Ooi – Institute of Climate Change, Universiti Kebangsaan Malaysia, Bangi, Selangor 43600, Malaysia; orcid.org/0000-0002-3325-0386

Ling Huang – Key Laboratory of Organic Compound Pollution Control Engineering (MOE), School of Environmental and Chemical Engineering, Shanghai University, Shanghai 200444, China

Cheng Huang — Shanghai Environmental Monitoring Centre, Shanghai 200235, China; orcid.org/0000-0001-9518-3628

Mohd Talib Latif — Department of Earth Sciences and Environment, Faculty of Science and Technology, Universiti Kebangsaan Malaysia, Bangi, Selangor 43600, Malaysia; orcid.org/0000-0003-2339-3321

Joshua S. Fu — Department of Civil and Environmental Engineering, University of Tennessee, Knoxville, Tennessee 37996, United States; oorcid.org/0000-0001-5464-9225

Complete contact information is available at: https://pubs.acs.org/10.1021/acsestair.5c00130

Author Contributions

L. Li. designed the study. Z.X. Sun. analyzed the data, performed the model simulations, and drafted the paper with contributions from all coauthors. J.T. Huo and C. Huang conducted field measurement and observational data analysis. M. Othman, Y.J. Wang, M. C.G. Ooi, L. Huang, M.T. Latif, and J.S. Fu contributed to data analysis and discussions. L. Li,

J.N. Tan, M.T. Latif, and J.S. Fu edited and reviewed the paper. All authors contributed to discussions of the paper.

Notes

The authors declare no competing financial interest.

ACKNOWLEDGMENTS

This study is financially supported by the Shanghai International Science and Technology Cooperation Fund (24230740200) and Shanghai Pujiang Program (23PJ1403100). This work is supported by Shanghai Technical Service Center of Science and Engineering Computing, Shanghai University.

REFERENCES

- (1) Huangfu, P.; Atkinson, R. Long-term exposure to NO₂ and O₃ and all-cause and respiratory mortality: A systematic review and meta-analysis. *Environ. Int.* **2020**, *144*, 105998.
- (2) Ainsworth, E. A.; Yendrek, C. R.; Sitch, S.; Collins, W. J.; Emberson, L. D. The Effects of Tropospheric Ozone on Net Primary Productivity and Implications for Climate Change. In *Annual Review of Plant Biology*, Merchant, S. S., Ed., 2012; Vol. 63, pp 637–661. DOI:
- (3) Feng, Z.; Xu, Y.; Kobayashi, K.; Dai, L.; Zhang, T.; Agathokleous, E.; Calatayud, V.; Paoletti, E.; Mukherjee, A.; Agrawal, M.; et al. Ozone pollution threatens the production of major staple crops in East Asia. *Nat. Food* **2022**, 3 (1), 47–56.
- (4) Krzyzanowski, M.; Cohen, A. Update of WHO air quality guidelines. *Air Qual., Atmos. Health* **2008**, *1* (1), 7–13.
- (5) Atkinson, R. Atmospheric chemistry of VOCs and NOx. Atmos. Environ. 2000, 34 (12–14), 2063–2101.
- (6) Liu, G.; Ma, X.; Li, W.; Chen, J.; Ji, Y.; An, T. Pollution characteristics, source appointment and environmental effect of oxygenated volatile organic compounds in Guangdong-Hong Kong-Macao Greater Bay Area: Implication for air quality management. *Sci. Total Environ.* **2024**, *919*, 170836.
- (7) Liu, Y. M.; Wang, T. Worsening urban ozone pollution in China from 2013 to 2017-Part 2: The effects of emission changes and implications for multi-pollutant control. *Atmos. Chem. Phys.* **2020**, *20* (11), 6323–6337.
- (8) Ivatt, P. D.; Evans, M. J.; Lewis, A. C. Suppression of surface ozone by an aerosol-inhibited photochemical ozone regime. *Nat. Geosci.* **2022**, *15* (7), 536–540.
- (9) Tan, Y.; Zhang, Y.; Wang, T.; Chen, T.; Mu, J.; Xue, L. Dissecting Drivers of Ozone Pollution during the 2022 Multicity Lockdowns in China Sheds Light on Future Control Direction. *Environ. Sci. Technol.* **2024**, *58*, 6988.
- (10) Le, T.; Wang, Y.; Liu, L.; Yang, J.; Yung, Y. L.; Li, G.; Seinfeld, J. H. Unexpected air pollution with marked emission reductions during the COVID-19 outbreak in China. *Science* **2020**, *369* (6504), 702–706.
- (11) Huang, X.; Ding, A.; Gao, J.; Zheng, B.; Zhou, D.; Qi, X.; Tang, R.; Wang, J.; Ren, C.; Nie, W.; et al. Enhanced secondary pollution offset reduction of primary emissions during COVID-19 lockdown in China. *Natl. Sci. Rev.* **2021**, *8* (2), nwaa137.
- (12) Sicard, P.; De Marco, A.; Agathokleous, E.; Feng, Z.; Xu, X.; Paoletti, E.; Rodriguez, J. J. D.; Calatayud, V. Amplified ozone pollution in cities during the COVID-19 lockdown. *Sci. Total Environ.* **2020**, 735, 139542.
- (13) Zhu, J.; Chen, L.; Liao, H.; Yang, H.; Yang, Y.; Yue, X. Enhanced PM_{2.5} Decreases and O₃ Increases in China During COVID-19 Lockdown by Aerosol-Radiation Feedback. *Geophys. Res. Lett.* **2021**, 48 (2), No. e2020GL090260.
- (14) Menut, L.; Bessagnet, B.; Siour, G.; Mailler, S.; Pennel, R.; Cholakian, A. Impact of lockdown measures to combat Covid-19 on air quality over western Europe. *Sci. Total Environ.* **2020**, 741, 140426.

- (15) Tan, Y.; Wang, T. What caused ozone pollution during the 2022 Shanghai lockdown? Insights from ground and satellite observations. *Atmos. Chem. Phys.* **2022**, 22 (22), 14455–14466.
- (16) Wang, Q.; Li, Y.; Zhong, F.; Wu, W.; Zhang, H.; Wang, R.; Duan, Y.; Fu, Q.; Li, Q.; Wang, L.; et al. Ground ozone rise during the 2022 shanghai lockdown caused by the unfavorable emission reduction ratio of nitrogen oxides and volatile organic compounds. *Atmos. Environ.* 2025, 340, 120851.
- (17) Zhang, Y.; Fu, Q.; Wang, T.; Huo, J.; Cui, H.; Mu, J.; Tan, Y.; Chen, T.; Shen, H.; Li, Q.; et al. A quantitative analysis of causes for increasing ozone pollution in Shanghai during the 2022 lockdown and implications for control policy. *Atmos. Environ.* **2024**, 326, 120469.
- (18) Zhu, J.; Wang, S.; Gu, C.; Jiang, Z.; Zhang, S.; Xue, R.; Yan, Y.; Zhou, B. Why Did Ozone Concentrations Increase During Shanghai's Static Management? A Statistical and Radical Chemistry Perspective. *Ecosphere* **2023**, 2023, 1–16.
- (19) Zhang, K.; Liu, Z.; Zhang, X.; Li, Q.; Jensen, A.; Tan, W.; Huang, L.; Wang, Y.; de Gouw, J.; Li, L. Insights into the significant increase in ozone during COVID-19 in a typical urban city of China. *Atmos. Chem. Phys.* **2022**, 22 (7), 4853–4866.
- (20) Shen, S.; He, L.; Chen, W.; Chen, S.; Ma, W. Spatial and Temporal Distribution Characteristics of Ozone Concentration and Source Analysis during the COVID-19 Lockdown Period in Shanghai. *Atmosphere* **2023**, *14* (10), 1563.
- (21) Dou, X.; Li, M.; Jiang, Y.; Song, Z.; Li, P.; Yu, S. Different contributions of meteorological conditions and emission reductions to the ozone pollution during Shanghai's COVID-19 lockdowns in winter and spring. *Atmos. Pollut. Res.* **2024**, *15* (10), 102252.
- (22) Jain, P.; Castellanos-Acuna, D.; Coogan, S. C. P.; Abatzoglou, J. T.; Flannigan, M. D. Observed increases in extreme fire weather driven by atmospheric humidity and temperature. *Nat. Clim. Change* **2022**, *12* (1), 63.
- (23) Huestis, D. L.; Dao, A.; Diallo, M.; Sanogo, Z. L.; Samake, D.; Yaro, A. S.; Ousman, Y.; Linton, Y.-M.; Krishna, A.; Veru, L.; et al. Windborne long-distance migration of malaria mosquitoes in the Sahel. *Nature* **2019**, *574* (7778), 404–408.
- (24) Garces, H.; Sbarbaro, D. Outliers detection in environmental monitoring databases. *Eng. Appl. Artif. Intell.* **2011**, 24 (2), 341–349. (25) Junninen, H.; Niska, H.; Tuppurainen, K.; Ruuskanen, J.;
- (25) Junninen, H.; Niska, H.; Tuppurainen, K.; Ruuskanen, J.; Kolehmainen, M. Methods for imputation of missing values in air quality data sets. *Atmos. Environ.* **2004**, *38* (18), 2895–2907.
- (26) Gettelman, A.; Mills, M. J.; Kinnison, D. E.; Garcia, R. R.; Smith, A. K.; Marsh, D. R.; Tilmes, S.; Vitt, F.; Bardeen, C. G.; McInerny, J.; et al. The Whole Atmosphere Community Climate Model Version 6 (WACCM6). *J. Geophys. Res. Atmos.* **2019**, *124* (23), 12380–12403.
- (27) Li, M.; Liu, H.; Geng, G. N.; Hong, C. P.; Liu, F.; Song, Y.; Tong, D.; Zheng, B.; Cui, H. Y.; Man, H. Y.; et al. Anthropogenic emission inventories in China: a review. *Natl. Sci. Rev.* **2017**, *4* (6), 834–866.
- (28) An, J. Y.; Huang, Y. W.; Huang, C.; Wang, X.; Yan, R. S.; Wang, Q.; Wang, H. L.; Jing, S. A.; Zhang, Y.; Liu, Y. M.; et al. Emission inventory of air pollutants and chemical speciation for specific anthropogenic sources based on local measurements in the Yangtze River Delta region, China. *Atmos. Chem. Phys.* **2021**, 21 (3), 2003–2025.
- (29) Huang, L.; Wang, Q.; Wang, Y.; Emery, C.; Zhu, A.; Zhu, Y.; Yin, S.; Yarwood, G.; Zhang, K.; Li, L. Simulation of secondary organic aerosol over the Yangtze River Delta region: The impacts from the emissions of intermediate volatility organic compounds and the SOA modeling framework. *Atmos. Environ.* **2021**, 246, 118079.
- (30) Huang, L.; Zhang, X.; Emery, C.; Mu, Q.; Yarwood, G.; Zhai, H.; Sun, Z.; Xue, S.; Wang, Y.; Fu, J. S.; et al. Recommendations on benchmarks for chemical transport model applications in China—Part 2: Ozone and Uncertainty Analysis. *Ecosphere* **2024**, 1–20.
- (31) Huang, L.; Zhu, Y. H.; Zhai, H. H.; Xue, S. H.; Zhu, T. Y.; Shao, Y.; Liu, Z. Y.; Emery, R.; Yarwood, R.; Wang, Y. J.; et al. Recommendations on benchmarks for numerical air quality model

- applications in China Part 1: $PM_{2.5}$ and chemical species. Atmos. Chem. Phys. 2021, 21 (4), 2725–2743.
- (32) Emery, C.; Tai, E. Enhanced Meteorological Modeling and Performance Evaluation for Two Texas Ozone Episodes, 2001.
- (33) Sillman, S.; He, D. Some theoretical results concerning O_3 -NO_x-VOC chemistry and NO_x-VOC indicators. *J. Geophys. Res. Atmos.* **2002**, 107 (D22), ACH 26-1.
- (34) Li, L.; Chen, C.; Huang, C.; Huang, H.; Zhang, G.; Wang, Y.; Chen, M.; Wang, H.; Chen, Y.; Streets, D. G.; et al. Ozone sensitivity analysis with the MMS-CMAQ modeling system for Shanghai. *J. Environ. Sci.* **2011**, 23 (7), 1150–1157.
- (35) Wang, Z.; Shi, C. N.; Zhang, H.; Ji, X. G.; Zhu, Y. Z.; Xia, C. Z.; Sun, X. Y.; Lin, X. F.; Yan, S. W.; Wang, S. Y.; et al. Opposing trends in the peak and low ozone concentrations in eastern China: anthropogenic and meteorological influences. *Atmos. Chem. Phys.* **2025**, 25 (1), 347–366.
- (36) Xing, J.; Wang, J.; Mathur, R.; Wang, S.; Sarwar, G.; Pleim, J.; Hogrefe, C.; Zhang, Y.; Jiang, J.; Wong, D. C.; et al. Impacts of aerosol direct effects on tropospheric ozone through changes in atmospheric dynamics and photolysis rates. *Atmos. Chem. Phys.* **2017**, *17* (16), 9869–9883.
- (37) Wang, J.; Allen, D. J.; Pickering, K. E.; Li, Z.; He, H. Impact of aerosol direct effect on East Asian air quality during the EAST-AIRE campaign. *J. Geophys. Res. Atmos.* **2016**, *121* (11), 6534–6554.
- (38) Zhu, J.; Chen, L.; Liao, H.; Yang, H.; Yang, Y.; Yue, X. Enhanced PM_{2.5} Decreases and O₃ Increases in China During COVID-19 Lockdown by Aerosol-Radiation Feedback. *Geophys. Res. Lett.* **2021**, 48 (2), No. e2020GL090260.
- (39) Zhao, X.; Zhang, Z.; Xu, J.; Gao, J.; Cheng, S.; Zhao, X.; Xia, X.; Hu, B. Impacts of aerosol direct effects on PM_{2.5} and O₃ respond to the reductions of different primary emissions in Beijing-Tianjin-Hebei and surrounding area. *Atmos. Environ.* **2023**, 309, 119948.
- (40) Langenbrunner, B.; Pritchard, M. S.; Kooperman, G. J.; Randerson, J. T. Why Does Amazon Precipitation Decrease When Tropical Forests Respond to Increasing CO₂? *Earths Future* **2019**, 7 (4), 450–468.
- (41) Wang, Y. J.; Yaluk, E. A.; Chen, H.; Jiang, S.; Huang, L.; Zhu, A. S.; Xiao, S. L.; Xue, J.; Lu, G. B.; Bian, J. T.; et al. The Importance of NOx Control for Peak Ozone Mitigation Based on a Sensitivity Study Using CMAQ-HDDM-3D Model During a Typical Episode Over the Yangtze River Delta Region, China. *J. Geophys. Res. Atmos.* 2022, 127 (19), No. e2022[D036555.
- (42) Li, X.; Qin, M.; Li, L.; Gong, K.; Shen, H.; Li, J.; Hu, J. Examining the implications of photochemical indicators for O₃–NOx–VOC sensitivity and control strategies: a case study in the Yangtze River Delta (YRD), China. *Atmos. Chem. Phys.* **2022**, 22 (22), 14799–14811.
- (43) Yang, Y.; Zhou, Y.; Wang, H.; Li, M.; Li, H.; Wang, P.; Yue, X.; Li, K.; Zhu, J.; Liao, H. Meteorological characteristics of extreme ozone pollution events in China and their future predictions. *Atmos. Chem. Phys.* **2024**, 24 (2), 1177–1191.
- (44) Chen, H.; Zhuang, B.; Liu, J.; Wang, T.; Li, S.; Xie, M.; Li, M.; Chen, P.; Zhao, M. Characteristics of ozone and particles in the near-surface atmosphere in the urban area of the Yangtze River Delta, China. *Atmos. Chem. Phys.* **2019**, *19* (7), 4153–4175.
- (45) Yue, M.; Wang, M.; Guo, J.; Zhang, H.; Dong, X.; Liu, Y. Long-Term Trend Comparison of Planetary Boundary Layer Height in Observations and CMIP6 Models over China. *J. Clim.* **2021**, *34* (20), 8237–8256.
- (46) Gu, J.; Zhang, Y.; Yang, N.; Wang, R. Diurnal variability of the planetary boundary layer height estimated from radiosonde data. *Earth Planet Phys.* **2020**, *4* (5), 1–14.
- (47) Myhre, G. Consistency Between Satellite-Derived and Modeled Estimates of the Direct Aerosol Effect. *Science* **2009**, 325 (5937), 187–190.
- (48) Cheng, Y.; Liu, C.; Wang, J.; Wang, J.; Zhang, Z.; Chen, L.; Ge, D.; Zhu, C.; Wang, J.; Ding, A. An observation-constrained estimation of brown carbon aerosol direct radiative effects. *Atmos. Chem. Phys.* **2024**, *24* (5), 3065–3078.

- (49) Gen, M.; Zhang, R.; Huang, D. D.; Li, Y.; Chan, C. K. Heterogeneous Oxidation of SO₂ in Sulfate Production during Nitrate Photolysis at 300 nm: Effect of pH, Relative Humidity, Irradiation Intensity, and the Presence of Organic Compounds. *Environ. Sci. Technol.* **2019**, 53 (15), 8757–8766.
- (50) Qu, Y.; Voulgarakis, A.; Wang, T.; Kasoar, M.; Wells, C.; Yuan, C.; Varma, S.; Mansfield, L. A study of the effect of aerosols on surface ozone through meteorology feedbacks over China. *Atmos. Chem. Phys.* **2021**, 21 (7), 5705–5718.
- (51) You, Q. L.; Cai, Z. Y.; Wu, F. Y.; Jiang, Z. H.; Pepin, N.; Shen, S. S. P. Temperature dataset of CMIP6 models over China: evaluation, trend and uncertainty. *Clim. Dyn.* **2021**, *57* (1–2), 17–35.

